Progressive failure of a repository drift in clay shale (PF experiment, Mont Terri Project)

Martin Ziegler[1*^], Markus Furche[2], Thies Beilecke[2], Anne Obermann[3], Simon Loew[4]

[1] Swiss Federal Office of Topography (swisstopo), Mont Terri URL, St.-Ursanne, Switzerland
[2] Federal Institute for Geosciences and Natural Resources, Hannover, Germany
[3] Swiss Seismological Service, Zurich, Switzerland
[4] Swiss Federal Institute of Technology, Zurich, Switzerland

* Corresponding author information: martin.ziegler@swisstopo.ch, +41 79 930 71 96
^ Presenting author

1. Introduction

Tectonic fault zones with vertical offsets < 20 m at depth levels of a nuclear waste repository (400–800 mbgs) cannot be predicted precisely nor completely from seismic measurements carried out at the ground surface prior to repository excavation. Excavating repository drifts or access tunnels into such faults at acute angles may lead to deep rock mass damage related to large tunnel caving/overbreak in the order of 1–3 tunnel diameters. Such zones are not only critical for short-term stability of an excavation in Opalinus Clay shale but could substantially reduce the effective thickness of the geological barrier and affect long-term safety. This may lead to abandoning of repository drift sections for waste disposal, and consequently to an increase of required subsurface footprint area for a high-level waste repository. In low-permeability clay shales structurally-controlled failure is initiated during excavation and damage of the geological barrier is expected to develop progressively over decades to thousands of years driven by hydromechanically and thermo-mechanically coupled processes and deterioration of tunnel support systems. Thus, it is important to evaluate fault zone hazard scenarios related to repository construction and long-term safety (Ziegler & Loew 2020).

The PF experiment explores structurally-controlled damage evolution in faulted Opalinus Clay shale in a 1:5 scale in-situ experiment at the Mont Terri URL, which is the topic of this paper. Additional works in the frame of the PF experiment include discontinuum simulations of short-term (experiment borehole drilling under undrained conditions) and longer-term (progressive failure evolution under partial desaturation) failure behavior (Zhao et al., this volume), as well as laboratory fault shear experiments. Here we present the in-situ experiment layout and first datasets.

2. In-situ Methods

The experiment consists of a 0.6 m wide and 12.9 m long, central experiment borehole, representing a repository drift at 1:5 scale, and six monitoring boreholes (Figure 1). The unsupported experiment and cased monitoring boreholes dissect a rock mass with different degree of tectonic fracturing and a major fault zone delineated by high-resolution (0.2 mm) optical imaging. We control the experiment borehole's relative air humidity (RH) and temperature to simulate open and closed drift phases, i.e., in a first phase we set the RH to approximately 65%, while in a second phase the RH will increase naturally by resaturation of the closed borehole. Ventilation causes the rock mass to desaturate over time, which we monitor with four sensors installed in slim, radial boreholes inside the experiment borehole up to a maximum depth of 24 cm. In addition, the rock mass state and evolution of rock mass damage are monitored by manifold techniques, including novel photogrammetric surveys of the experiment borehole, active seismic and electrical resistivity single-hole and cross-hole tomographic imaging, as well as recordings of pico-seismicity, aiming at exploring and localizing macro- and microscopic damage propagation evolving in the crown of the experiment borehole. Considering seismic acquisitions, we conduct 2–3 surveys using borehole sondes per year that yield with high spatial resolution, daily acquisitions with permanently installed sensors but of lower spatial resolution, and continuous monitoring of picoseismicity (acoustic emissions). Technical setups and processing techniques are given in Ziegler & Loew (2021) and Ziegler et al. (2022). At present, the experiment is in the ventilation phase, where the rock surrounding the experiment borehole strengthens due to desaturation and associated suction but also fractures due to desiccation. Before entering the resaturation phase, in which we expect rock strength reduction that may lead to increasing damages, additional fiber optic strain sensors will be installed to monitor fracture displacements along the borehole wall that we will compare with photogrammetric data.

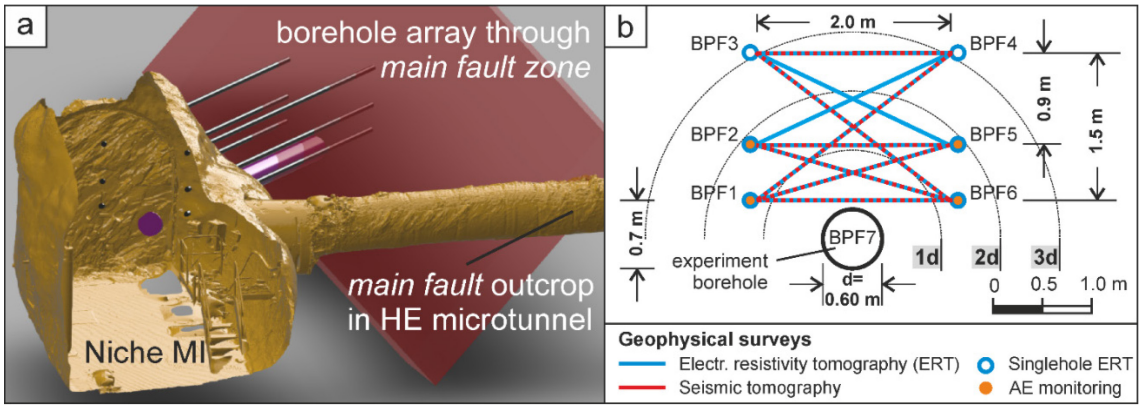

Figure 1. (a) Niche MI of the Mont Terri URL with the PF experiment borehole array that intersects a major fault zone. (b) 2D sketch of the PF tomographic monitoring (BPF-1–6) and experiment borehole (BPF-7) array. We record the evolution of macroscopic overbreak formation using photogrammetry inside the experiment borehole. Changes of rock mass state properties and damage are explored by acoustic and electric tomographic monitoring techniques. Modified after Ziegler & Loew (2021).

3. Results

3.1. Environmental monitoring

Throughout 2021, the relative humidity (RH) of the experiment borehole was controlled and set to 65±2% (Figure 2). The temperature remained in a narrow band (17.5–19°C) over the same period. At a depth of 3.6–3.8 m TBC (top borehole casing), we measured equilibrated air humidity in slim, 1–24 cm deep, radial boreholes. The monitoring site locates at a slightly fractured but stable portion of the borehole. The shallowest interval (1–4 cm) indicated rock desaturation starting from October 28th, 2020, while the 6–9 cm and 12–15 cm deep intervals indicated delayed desaturation starting on November 30th, 2020 and June 18th, 2021, respectively. The deepest interval at 21–24 cm depth remained fully saturated (Figure 2). The first three intervals did not yet reach steady-state conditions. In order to quantify the extracted borehole moisture from BPF-7 we started measuring the air outflow rate from October 2021, additional to the extracted air moisture and temperature that we recorded over the entire time period.

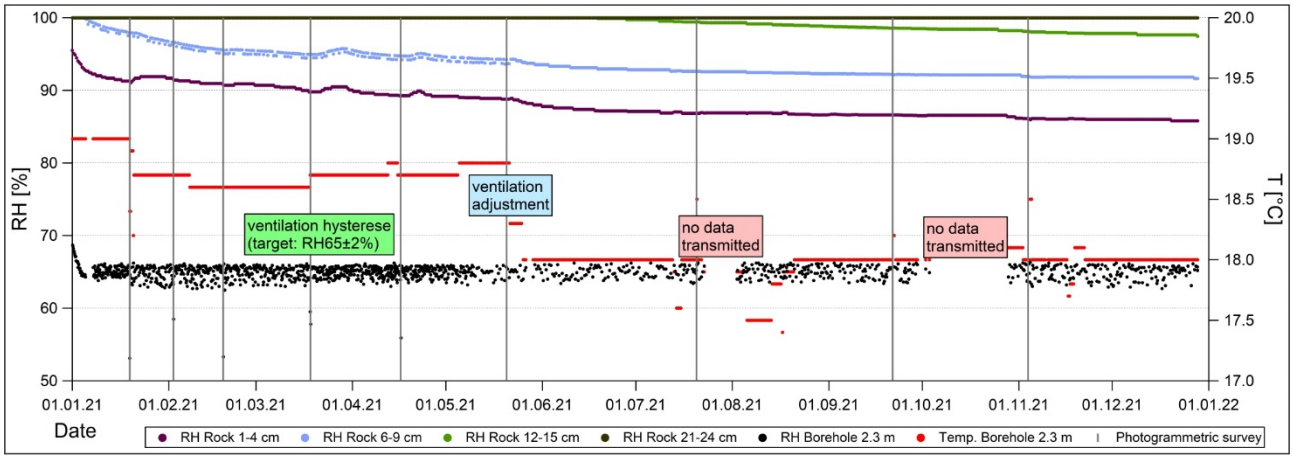

Figure 2. Evolution of relative humidity (RH) and temperature (T) inside the experiment borehole. Decreases of RH inside 3-cm-long intervals in slim, radial boreholes indicate rock desaturation (Ziegler et al. 2022).

3.2. Fracture analyses

We identified twenty-four tectonic structures along the experiment borehole from unwrapped borehole wall images (Figure 3a). As in most monitoring boreholes, the major fault zone has sharp upper and lower boundaries, is rich in scaly clay, and shows a few mm thick, dark layer of fault gouge of slightly different orientation than the fault zone's average orientation (Figure 3b,d). The majority of discrete fault planes (fault set 1) in the hanging wall and footwall rock mass are subparallel to the main fault zone and to rock bedding (Figure 3c). A second set of faults (set 2) is gently dipping to the East.

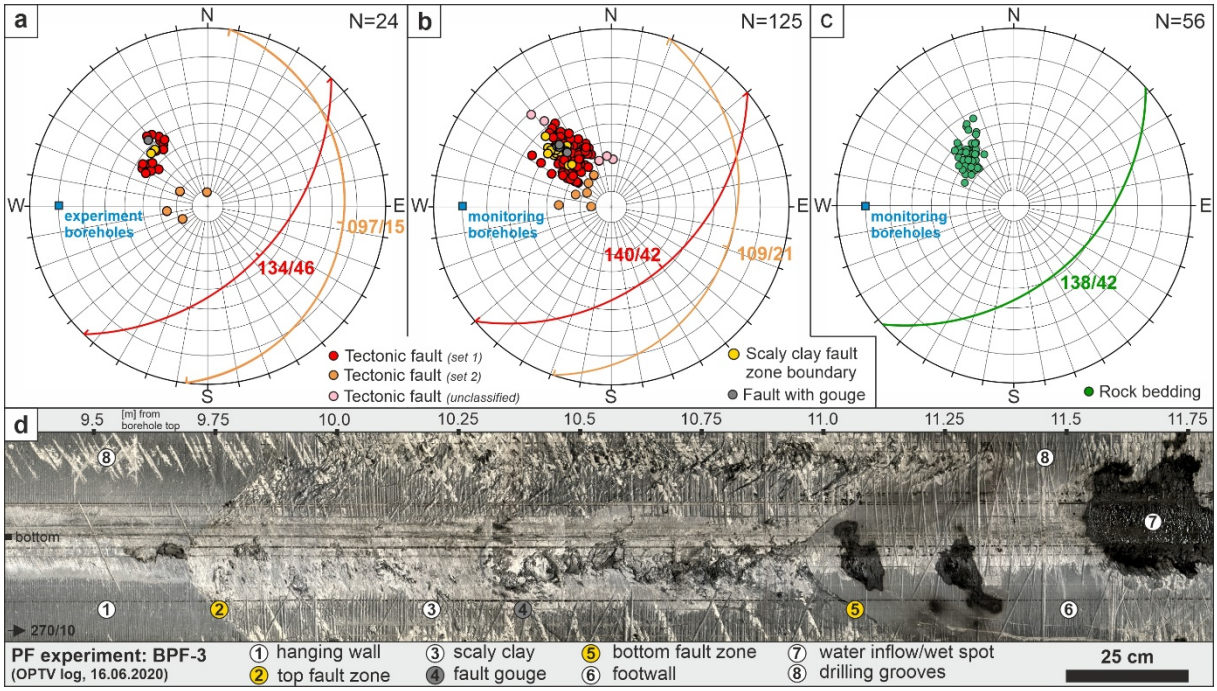

Figure 3. Pole points to tectonic faults encountered in (a) the experiment borehole and (b) the six monitoring boreholes. (c) Poles to bedding planes have similar orientation compared to tectonic joints of set 1. (d) Unrolled optical borehole wall image of BPF-3 showing fine details of the rock mass structure surrounding the major fault zone. Also water inflows that formed wet spots occurred.

Stress-induced borehole wall breakouts formed rapidly during the drilling of the experiment borehole (BPF-7) in likely saturated rock and then increased in size only slowly during the desaturation phase (Sutter 2021). Some breakout sections stabilised. We can explain this behaviour by the rapid stress field modification upon drilling causing stress concentrations that exceeded rock strength, which is weaker for saturated compared to desaturated Opalinus clay shale (Wild et al. 2015). Nevertheless, time-lapse borehole wall images show ongoing displacements in damage/overbreak zones and offsets along some tectonic faults, i.e., progressive failure. Within the first five weeks after drilling and the start of the ventilation, new sets of tensile fractures formed. The first set follows the orientation of bedding planes. The second set is roughly perpendicular to the borehole axis or dips steeply (>70°) toward North-East in some parts of the borehole. Sutter (2021) identified about 570 open fracture traces with a cumulative length of 24 m on the unrolled borehole wall image of October, 2020, and maximum numbers of traces of about 5,460 and 5,500 fractures (and cumulative lengths of 127 m and 128 m) on images of November, 2020. Later images between December 2020 and April, 2021, showed a slightly decreasing number of visibly open fractures from about 5,400 to 4,890 and decreased cumulative fracture lengths from 125 m to 118 m. The observations suggest that the ventilation process leads to the formation of shrinkage cracks that form and propagate soon after the start of the ventilation. The reduction of the number and cumulative lengths of fractures seen later may indicate hydro-mechanical processes causing fracture closure, e.g., as part of borehole convergence.

3.3. Preliminary data of tomographic surveys

As an example of the acquired electrical resistivity data, rock mass resistivity changes between December 2020 and April 2021 were calculated and are shown in Figure 4a as a relative change in the form of a ratio. In general, relatively small changes can be seen with a slight decrease in the resistivity being observed in the vertical plane of the three left-hand holes (BPF-1 to BPF-3). Noteworthy is the area of a relatively strong decrease in resistivity directly above the main borehole BPF-7 in the range between 9.5 m and 11.5 m, i.e., in the footwall of the major fault zone where wet spots were found in monitoring boreholes (Figure 3d). Figure 4b shows monthly recordings for two exemplary, stationary seismic transmitter-receiver couples from April to November 2021. While the first arriving waveforms remain very similar over the observation period, the later arriving coda waves show a gradual phase-shift that relates to an increase in seismic velocity. Besides the phase-shift, also an increase in amplitude can be observed. Tomographic data analysis and interpretation are ongoing.

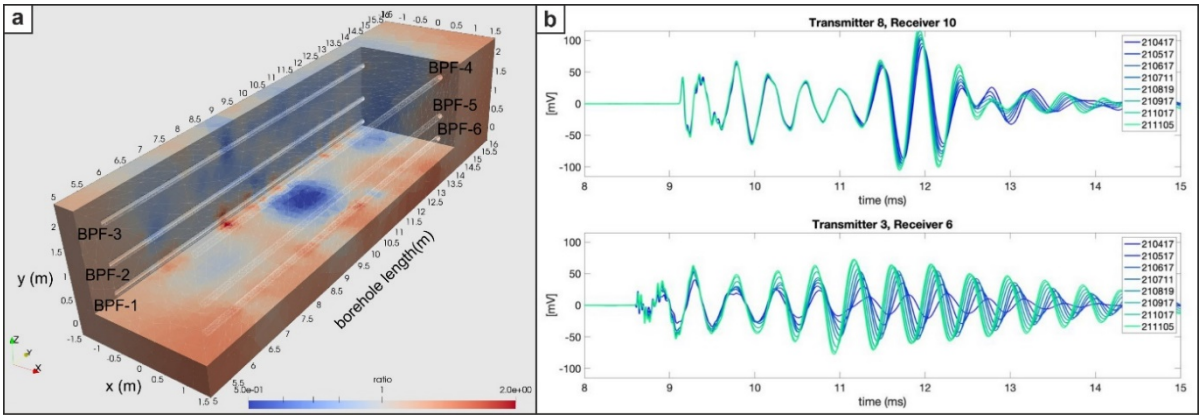

Figure 4. (a) Electrical resistivity (ρ) changes between December 2020 and April 2021 shown as a ratio. Blue colours represent decreases and red colours increases in ρ. (b) Examples of two transmitter-receiver couples with monthly recordings from April to November 2021. A phase-shift and an amplitude change in the later arriving coda waves are apparent. Taken from Ziegler et al. (2022).

4. Conclusions

We obtained manifold datasets to characterize the initial structures of the experiment rock mass as well as its state and structural changes over the first experiment phase, focusing on the effects of ventilation. On one side, the ventilation led to the formation of thousands of cm–dm long shrinkage fractures. The monitored zone of desaturation reached radially between about 15 cm and 21 cm deep into the rock formation. This suggests that desiccation fractures may be limited in their radial extent to few decimeters from the borehole wall but the fractures may propagate also into saturated rock portions and cause also deeper-reaching desaturation and related fracturing. On the other side, we argue that rock desaturation likely slowed down the measured extension of borehole overbreaks and deeper damage due to an increased rock strength of the Opalinus Clay shale. It is possible that monitored fracture closure in the near field of the experiment borehole and rock desaturation caused or at least contributed to the increase of amplitudes and the earlier arrivals of recorded coda waves. Substantial reductions in electrical resistivity may be caused by drainage of water in fractures, which requires more in depth assessment. Note that water inflows in the form of wet spots along faults were detected in monitoring boreholes.

The PF in-situ experiment generates comprehensive data sets on the initial state and evolution of rock mass structural and physical properties associated with short- and long-term hydromechanical processes. The first analyses are promising with regard to the data quality and highlight complex, hydromechanically coupled processes. In the next project phase, we will extend our data analyses and compare the evolution of different rock mass properties (structural, deformation, seismic, electrical resistivity data sets) expecting valuable insights into faulted Opalinus Clay rock mass behavior and its damage evolution during different humidity boundary conditions.

5. Acknowledgments

The Swiss Federal Nuclear Safety Inspectorate (ENSI) and the Swiss Federal Office of Topography (swisstopo) are funding the PF experiment led by the Chair of Engineering Geology at ETH Zurich. The Swiss Seismological Service (SED) and the Federal Institute for Geosciences and Natural Resources (BGR) in Germany conducted electrical resistivity tomography, active as well as passive seismic tomography surveys in monitoring boreholes. We are very grateful for their essential contributions. The institutions are formal partners of the Mont Terri Project Consortium.

6. Reference list

Sutter, E. 2021. Progressive failure and deformation analysis of a large-diameter experiment borehole. B.Sc. thesis, Department of Earth Sciences, ETH Zurich, 40 pp.

Wild, K, Wymann, LP, Zimmer, S, Thoeny, R, Amann, F. 2015. Water retention characteristics and state-dependent mechanical and petro-physical properties of clay shale. Rock Mechanics and Rock Engineering, 48, 427–439.

Ziegler, M, Loew, S. 2020. Mont Terri PF experiment: Progressive failure of structurally-controlled overbreaks — Project introduction and overview of work program. ENSI Research and Experience Report 2019, ENSI-AN-10919, 307–315.

Ziegler, M, Loew, S. 2021. PF-Experiment: Installation and first data. Mont Terri Technical Note 2020-37, 15 pp.

Ziegler, M, Lei, Q, Zhao, C, Moradian, O, Obermann, A, Furche, M, Beilecke, T, Loew, S (2022, in press). Mont Terri PF Experiment: Progressive Failure of Structurally Controlled Overbreaks — Status update 2021. ENSI Research and Experience Report 2021, 10 pp.